Geophysical Research Letters

RESEARCH LETTER
10.1029/2022GL102133

Key Points:

- Shipboard and satellite gravity data were used to explore the crustal structure in the Galapagos triple junction region
- The gravity-derived crustal thickness with a standard thermal model does not appear to be realistic in this region
- A simple smoothing filter applied to the standard thermal model could explain gravity variation along the Cocos-Nazca spreading center

Supporting Information:

Supporting Information may be found in the online version of this article.

Correspondence to:

T. Zheng and J. Lin,
tzheng@scsio.ac.cn;
jianlin@scsio.ac.cn

Citation:

Zheng, T., Lin, J., Schouten, H., Smith, D. K., Klein, E., & Parnell-Turner, R. (2023). Gravity anomalies and implications for shallow mantle processes of the western Cocos-Nazca spreading center. *Geophysical Research Letters*, *50*, e2022GL102133. https://doi.org/10.1029/2022GL102133

Received 5 DEC 2022
Accepted 14 FEB 2023

Author Contributions:

Conceptualization: Hans Schouten
Funding acquisition: Hans Schouten
Methodology: Tingting Zheng, Jian Lin
Resources: Ross Parnell-Turner
Software: Tingting Zheng
Supervision: Jian Lin
Writing – original draft: Tingting Zheng
Writing – review & editing: Tingting Zheng, Jian Lin, Hans Schouten, Deborah K. Smith, Emily Klein, Ross Parnell-Turner

Gravity Anomalies and Implications for Shallow Mantle Processes of the Western Cocos-Nazca Spreading Center

Tingting Zheng[1,2], Jian Lin[1,3], Hans Schouten[4], Deborah K. Smith[4], Emily Klein[5], and Ross Parnell-Turner[6]

[1]China Key Laboratory of Ocean and Marginal Sea Geology, South China Sea Institute of Oceanology, Innovation Academy of South China Sea Ecology and Environmental Engineering, Chinese Academy of Sciences, Guangzhou, China, [2]China-Pakistan Joint Research Center on Earth Sciences, CAS-HEC, Islamabad, Pakistan, [3]Department of Ocean Science and Engineering, Southern University of Science and Technology, Shenzhen, China, [4]Department of Geology and Geophysics, Woods Hole Oceanographic Institution, Woods Hole, MA, USA, [5]Duke University, Durham, NC, USA, [6]Scripps Institution of Oceanography, University of California, San Diego, La Jolla, CA, USA

Abstract This study analyzes up-to-date gravity data in the Galapagos triple junction region to understand crustal structure and melt distribution beneath the propagating Cocos-Nazca spreading center (CNSC). Application of a standard thermal model to the mantle Bouguer gravity anomaly (MBA) does not appear to result in a realistic crustal thickness in this region. The cross-CNSC MBA profiles flatten and axial values increase from east toward the western end of the CNSC. A simple smoothing filter applied to the standard thermal model with different filter widths can explain the progressive flattening of the MBA and is interpreted as different distribution widths (concentrations) of partial melt in the mantle. The east-west residual MBA gradient along the CNSC is similar to the east flank of the East Pacific Rise (EPR), suggesting that the along-CNSC gradient could partly reflect the shallow mantle properties associated with the EPR.

Plain Language Summary This study investigates changes in crustal thickness and shallow mantle properties beneath the westward propagating Cocos-Nazca spreading center (CNSC) by analyzing shipboard gravity data combined with satellite gravity data in the Galapagos triple junction region. By assuming a general 1-D plate cooling model, we correct the age-induced thermal effect of the lithosphere with a standard thermal model, which suggest thinner crust near the western tip of the CNSC increasing in thickness toward the east. However, results also indicate that the crust continues to thicken from the CNSC axis to the north and south edges of the gore, which does not seem realistic. Instead, these gravity signals most likely reflect properties within the shallow mantle, specifically a eastward decrease in the width (and hence increase in concentration) of melt within the shallow mantle beneath the CNSC. The residual gravity gradient along the CNSC axis is similar to that on the east flank of the East Pacific Rise (EPR), suggesting that the CNSC axis gravity gradient could in part reflect variation in the mantle density beneath the EPR.

1. Introduction

At the Galapagos triple junction, the Cocos, Nazca, and Pacific plates surround the Galapagos microplate (GMP, Figure 1a). The westward propagation of the Cocos-Nazca spreading center (CNSC, spreading rate ~48.2 mm/yr) has formed the westward-pointing, V-shaped Galapagos gore, with large-relief scarps defining its edges (Holden & Dietz, 1972). The tip of the Galapagos gore is currently located ~25 km east of the East Pacific Rise (EPR) spreading axis (~128 mm/yr) (DeMets et al., 2010; Lonsdale, 1988; Schouten et al., 2008; Searle & Francheteau, 1986; Smith et al., 2011). North and south of the gore, incipient rift (IR) and Dietz volcanic ridge (DVR) intersect the EPR axis at 2°40′N and 1°12′N, respectively, forming two ridge-ridge-ridge triple junctions (Lonsdale, 1988; Schouten et al., 2008). The GMP formed south of the gore ca. 1.4 Ma and Dietz volcanic ridge forms its southern boundary (Searle & Francheteau, 1986).

Most previous studies in the area have focused on the kinematics of the triple junction region (e.g., Zonenshain et al., 1980; Searle & Francheteau, 1986; Lonsdale, 1988; Smith et al., 2013), the Hess Deep Rift (e.g., Francheteau et al., 1990; Gillis et al., 2014; Smith & Schouten, 2018; Stewart et al., 2002, 2003), the eastern CNSC, also called the Galapagos spreading center (e.g., Puchelt & Emmermann, 1983; Schilling et al., 1982, 2003; Sinton et al., 2003), and the Galapagos hotspot (e.g., Canales et al., 1997, 2002; Detrick et al., 2002; Ito & Lin, 1995a, 1995b; Ito et al., 1997; Lin & Phipps Morgan, 1992). To investigate the transition from rifting at

10.1029/2022GL102133

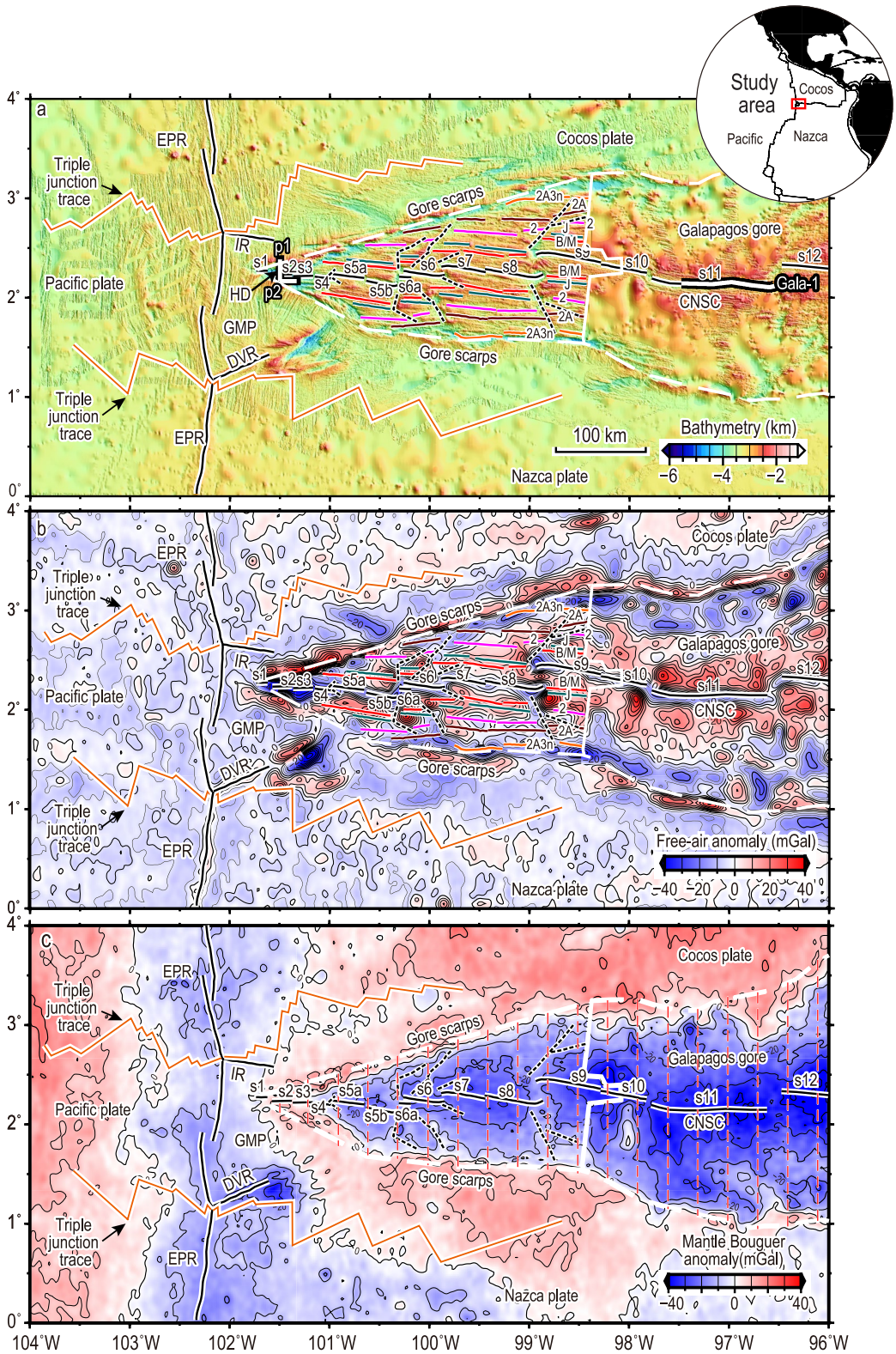

Figure 1.

the western end of the Galapagos gore to full magmatic spreading to the east, geophysical data were collected in the gore from ~101.7°W to ~98.5°W in 2018 (Smith et al., 2020). Spreading segments s1 to s12 identified in Figure 1a open in two spreading regimes: segments s1 to s3 open between Cocos and the Galapagos microplate at very slow spreading rates of 19–29 mm/yr (i.e., Cocos-Galapagos Spreading Center, CGSC) and represent the transition from rifting to magmatic spreading; segments s4 to s12 open between the Cocos and Nazca plate at 48.2 mm/yr (i.e., CNSC) and are spreading magmatically (Smith et al., 2020).

In this study, we examine the crustal structure of the Galapagos gore in the larger context of the Galapagos triple junction. We combine shipboard data of Smith et al. (2020) with previously collected shipboard bathymetric, free-air gravimetric, and magnetic data, as well as satellite data, and we calculate mantle Bouguer anomaly (MBA), residual mantle Bouguer anomaly (RMBA), and gravity-derived relative crustal thickness from 104°W to 96°W and from 0° to 4°N. Within the Galapagos gore itself we examine the patterns in the gravity data to obtain insight into the establishment of seafloor spreading at the CNSC in the wake of the westward propagating gore tip. We investigate trends in gravity along and across the axis of the CNSC. We propose a smoothed MBA model to explain the possible cause of gravity anomalies in this region.

2. Data and Analysis

2.1. Bathymetry

Multibeam bathymetric data from cruise SR1806 (https://www.rvdata.us/search/cruise/SR1806) were combined with data collected by previous multibeam surveys from the Global Multi-Resolution Topography (Ryan et al., 2009). Bathymetric depths estimated from satellite altimetry, gridded at 15 arc second node spacing, were used where multibeam bathymetry data were unavailable (Tozer et al., 2019). These data were merged into a grid with 100-m node spacing (Figure 1a).

2.2. Free-Air and Mantle Bouguer Gravity Anomalies

Shipboard free-air gravity anomaly (FAA) data were collected using a Bell Aerospace BGM-3 gravimeter (Smith et al., 2020), and merged with global satellite-derived gravity (Sandwell et al., 2014) (Figure 1b). We used the spectral method of Parker (1972) to calculate the mantle Bouguer anomaly (MBA) by removing the gravitational effects of the water-crust and crust-mantle interfaces from the FAA, assuming water, crust, and mantle densities of 1.03×10^3, 2.7×10^3, and 3.3×10^3 kg m^{-3}, respectively, and using a reference crustal thickness of 6 km (Figure 1c). The FAA and MBA were gridded at 1-arc-second node spacing.

We tested data resolution by comparing MBA calculated from satellite versus shipboard data. The results, as expected, show that using multibeam bathymetric and shipboard gravity data resolves more spatial features within the gore than using only satellite data or satellite gravity plus multibeam bathymetry (Figure S1 in Supporting Information S1).

2.3. Magnetic Anomalies and Crustal Age Model

Within the gore from ~101.7°W to ~98.5°W, magnetic anomalies were identified by Smith et al. (2020), and the anomalies were assigned ages based on the geomagnetic polarity timescale of Ogg (2012). Outside the gore, we used GPlates software (Müller et al., 2018) to generate 10-km-spaced flowlines and determine the crustal ages along these flowlines at 1-Myr intervals. Age perturbations within the GMP by tectonic rotation were ignored. Flowline ages were merged into a 2D grid with 1-arc-second spacing (Figure S2a in Supporting Information S1).

2.4. RMBA and Gravity-Derived Crustal Thickness

In our study area, the RMBA was calculated by subtracting age-dependent thermal effects from the MBA (Figure 2a). The age-induced thermal structure was estimated by assuming a 1-D plate cooling model (Turcotte

Figure 1. (a) Bathymetric data in the study region. The upper right inset shows the location of study area (red box), plate boundaries are from Bird (2003). Spreading segments s1 to s12 are identified along the CNSC. North and south of the Galapagos microplate (GMP), two triple-junction traces marked with red lines are from Schouten et al. (2008) and Smith et al. (2011). Solid black lines are ridge axes; dashed white lines mark the gore scarps; the solid white line marks the eastern end of Cruise SR1804 survey; colored lines within the gore identify isochrons as labeled; lines labeled p1, p2, and Gala-1 are seismic lines from Zonenshain et al. (1980) and Canales et al. (2002), respectively. HD: Hess Deep; IR: incipient rift; DVR: Dietz volcanic ridge. (b) Free-air gravity anomalies with a contour interval of 5 mGal. (c) Mantle Bouguer anomalies (MBA) with a contour interval of 10 mGal. Dashed red north-south lines indicate locations of profiles in Figure 3.

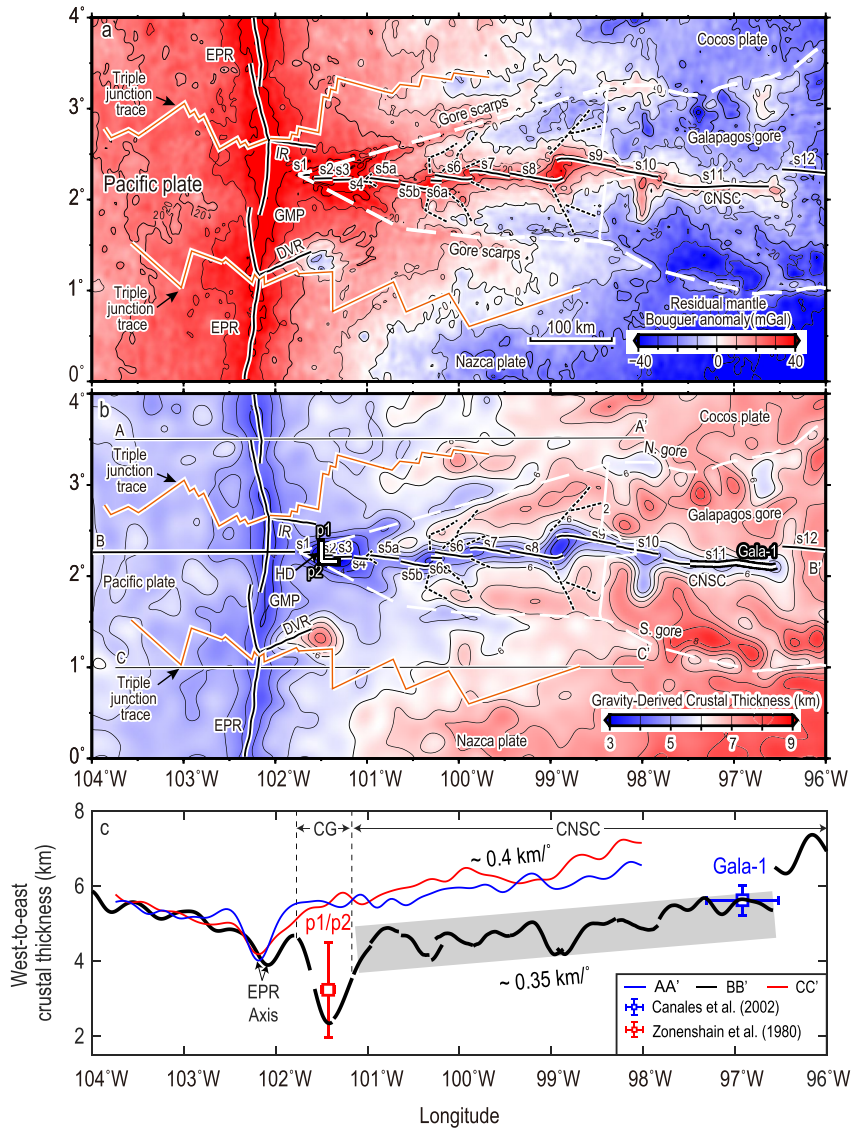

Figure 2. (a) Map of residual mantle Bouguer anomaly (RMBA) with a contour interval of 10 mGal; labeling as in Figure 1. The CNSC-generated crust within the Galapagos gore shows slightly less positive RMBA than the EPR-generated crust outside of the gore, except in the gore tip area (segments s1 to s3). (b) Gravity-derived crustal thickness derived from (a) with a 7.5 km shift to match seismic results from Zonenshain et al. (1980) and Canales et al. (2002). The contour interval is 0.5 km. West-east lines A-A' to C-C' locate profiles in (c). (c) West-east profiles noted in (b), showing crustal thickness across the EPR and along the CNSC. The tip area includes segments s1 to s3 (CG), where EPR crust is being rifted; the CNSC is spreading between the Cocos and Nazca plates. Gray bar shows the west-to-east crustal thickening trend along the CNSC. Note that the eastern flank of the EPR-generated crust follows a similar west-to-east crustal thickening trend (blue and red lines).

& Schubert, 2014; Wang et al., 2011), using standard parameters given by Wang et al. (2011) for the Mid-Atlantic region, which is considered to be the standard thermal model for lithospheric cooling.

Assuming that the RMBA is controlled only by variations in crustal thickness, an end-member model of the relative crustal thickness was calculated by the downward continuation of the RMBA to a depth of 10 km. Wang et al. (2011) tested different downward continuation depths for crustal thickness variations and found no significant differences in choosing depth. The relative crustal thickness was later shifted as a whole to match the seismic-determined crustal thickness along the CNSC (Figures 2b and 2c).

We note that RMBA reflects both density anomalies from the crust and mantle. Existing regional density or temperature anomalies from the shallow mantle could result in biases to our gravity-derived crustal thickness. In

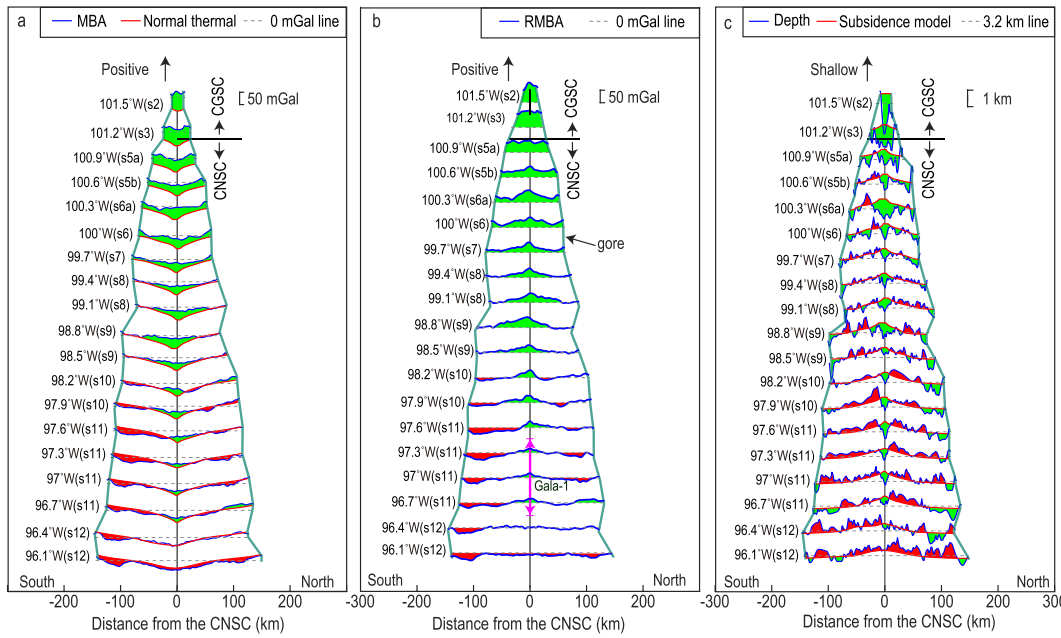

Figure 3. Cross-axis profiles of the CGSC and CNSC within the Galapagos gore, labeled by longitude and segment number. Profile locations are in Figure 1c; lines are at intervals of 0.3° longitude. (a) MBA (blue line) and standard thermal model (red line). Misfits between MBA and standard thermal model are filled with red and green. Light blue lines marks gore scarps. (b) RMBA calculated from standard thermal model. Green fill (elevated RMBA) implies thinner crust and red fill implies thicker crust. Arrow line locates seismic refraction line Gala-1 (Canales et al., 2002). (c) Bathymetry (blue lines) and subsidence calculated from standard thermal model (red lines). Misfits are emphasized by red and green fill.

addition, we used a 1-D simple standard thermal model for the MBA correction, which may also affect the final crustal thickness in the Galapagos triple junction region as the lithospheric cooling process of a triple junction may be different from the normal spreading Mid-Atlantic region.

3. Results

3.1. MBA, RMBA, and Crustal Depth

Our map of MBA shows two major features (Figure 1c): (a) As noted by Smith et al. (2020), the MBA decreases from west to east within the gore (∼10 mGal/°) and shows "Bull's eye" gravitational lows along segments s5a–s9; this pattern continues eastward through segments s10–s12. (b) Across the CNSC and on the flanks of the EPR, the MBA increases away from the spreading axis. A series of MBA profiles across the CNSC axis, extracted from west to east at intervals of 0.3° within the gore, are shown in Figure 3a and are compared with the standard thermal model (red lines) calculated from crustal age. MBA is shifted −10 mGal to improve visual comparison with the standard thermal model in all profiles throughout this study. We see considerable misfit between the MBA and the thermal model, especially in the western section of the gore (Figure 3a). The MBA loses more and more of its characteristic axial minimum from 96.4°W toward the west and increases and flattens toward segment s3. Consequently, the RMBA increases in value toward the gore tip (Figure 3b).

In contrast, the adjacent EPR shows relatively little variation in MBA and RMBA along the spreading axis, that is, the RMBA displays a relatively constant amplitude of 40 ± 5 mGal (Figure 2b). We see a clear regional high RMBA within a cross-axis width of 100–200 km (i.e., ∼2–3 Ma) on each flank of the EPR, indicating that the standard thermal model also does not fit the EPR flanks. Within the study region, Dietz seamount at the southern border of the GMP shows more negative values in MBA and RMBA (Figures 1a and 2b) than surrounding areas and can be described as a mini-hotspot (Smith et al., 2020).

In Figure 3c, we compare the bathymetry with a plate subsidence model with assumed axial depth of 2.6 km for the cross-axis lines shown in Figure 1c. Aside from the expected misfit between the axial valley and the predicted subsidence model at the CNSC, the main feature of this comparison is that off-axis seafloor depth is shallower

than predicted from the subsidence model in profiles, particularly in segments s5–s12 of the CNSC. The axial valley misfit decreases steadily eastward from the gore tip and is minimal in segment s12 near 96.1°W.

3.2. Gravity-Derived Crustal Thickness Results

3.2.1. Calibration of Gravity-Derived Relative Crustal Thickness With Seismic-Defined Crustal Thickness

To calibrate the gravity-derived relative crustal thickness, we compared our results with the seismically determined crustal thickness from two seismic surveys within the Galapagos gore, one near the gore tip (Zonenshain et al., 1980) and the other near 97°W (Canales et al., 2002) (Figure 2c). The Moho discontinuity identification in the seismic profiles of Zonenshain et al. (1980) is highly subjective because of poor-quality imaging and thus, we averaged the crustal thickness values obtained in profiles p1 and p2 to show the uncertainty. Our gravity-derived relative crustal thickness was shifted by 7.5 km to match the seismically determined crustal thickness of Canales et al. (2002) (Figures 2b and 2c).

3.2.2. Crustal Thickness Variation

Under the assumption that the RMBA only reflects the crustal thickness variation, gravity-derived relative crustal thickness is lowest along the axis of the EPR and along the axis of the CNSC, and this thickness appears to increase off-axis in both locations. On the CNSC, crustal thickness increases eastward by ∼0.35 km/° along segments s4–s9 within our study area and apparently more rapidly farther to the east through segment s12 (Figures 2b and 2c). We further examined the axial depth, which shoals by ∼0.19 km/° eastward in segments s4-s9 (Figure S3 in Supporting Information S1). On the EPR, crustal thickness is also thin at the axis, only 4 km, but does not vary substantially along the axis; crust thinner than ∼6 km extends ∼100–200 km from the EPR axis (Figure 2b). There are no seismic data to confirm this calculation results.

Two local areas adjacent to the GMP are associated with pronounced crustal thickness anomalies (Figure 2b). The first is the westernmost ∼75 km of the gore, which includes segments s1–s3 and shows a more positive RMBA (up to ∼65 mGal) and thinner crust (up to ∼2.4 km) than the surrounding area, consistent with the findings of Zonenshain et al. (1980). The second is Dietz seamount, which has thicker crust (up to ∼7.5 km) than the surrounding area.

4. Discussion

4.1. Gravity Variation and Implication

Our gravity analysis implies relatively thin crust along the axis of most segments (s1–s11) within the Galapagos gore and along the axis of the EPR (Figure 3a). At its western end, Galapagos gore crust is thinnest (∼2–4 km) and the zone of thin crust is widest at 101°W (∼75 km, or ∼1.5 m.y., Figure 2b); eastward, the crust thickens and the width of thin crust narrows to around 96°W where crust is a normal ∼6–7 km thick. This corresponds to an overall west-to-east shallowing of axial depth (∼0.19 km/°) and decreasing MBA and RMBA (∼10 mGal/°). At the EPR, the crust is thinnest (∼3–4 km) along the axis and the zone of thin crust is at least ∼200 km wide (∼2.5 m.y.) on each flank.

Progressive development of melt supply to more easterly magmatic segments at the CNSC might explain the thickening of the axial crust eastward from the gore tip. However, if this is the case, we expect thin crust near the gore scarps, that is, where rifting first developed in spreading segments, much like we presently observe at the axis of segments s4/s5. This is not observed. Similarly, the pattern observed at the EPR and its flank does not seem realistic. Because of this, we explore the possibility that some of the gravity signal is influenced by density variation in the shallow mantle.

4.2. MBA Flattening Patterns

From ∼96.4°W at the CNSC and continuing to the west, the MBA does not have a characteristic of sharp minimum at the ridge axis but instead becomes flatter, and the misfit with the age-based thermal model (green shading in Figure 3a) increases. This pattern causes the RMBA to increase in amplitude and width toward the west (Figure 3b). To explain this pattern, we simulate the flattening of the MBA by applying a simple smoothing filter

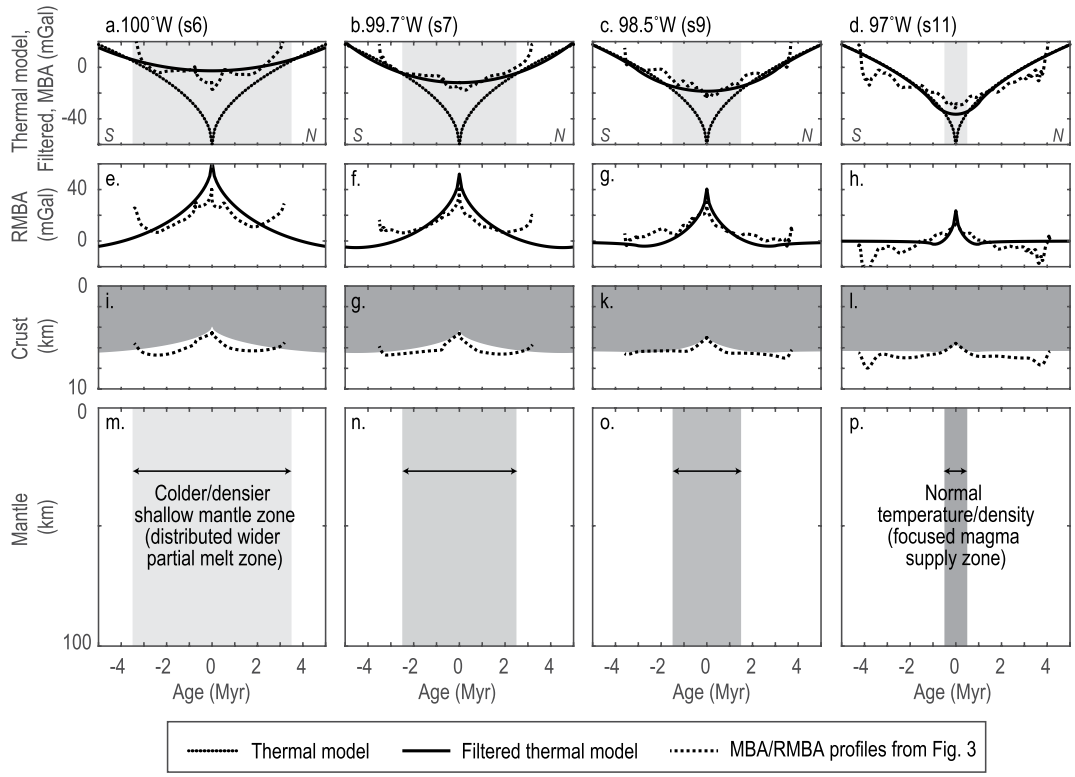

Figure 4. Filtered thermal models simulating west-to-east variation in CNSC MBA gravity. (a–d) Profiles at longitudes indicated at top show MBA (short-dashed lines) and standard thermal model (dotted). Filtered thermal models (solid lines) illustrate progressive east-to-west flattening of the sharp peak (gray zones) in the standard thermal model so as to match the observed MBA. (e–h) Model RMBA (solid lines) calculated using thermal model minus filtered thermal model and RMBA calculated from cross-CNSC profiles (short-dashed lines), showing a increasing trend in both amplitude and width. (i–l) Crustal thickness (gray) calculated from RMBA in panels (e–h) and from cross-CNSC profiles (short-dashed lines). (m–p) Schematic representation of a colder and denser shallow mantle zone, corresponds to a wider potential distributed partial melt zone, gradually evolves to a focused magma supply zone. This filter smoothes the standard thermal model as shown in panels (a–d).

to the thermal model. We use a square root function of age to represent the thermal model and smooth it at different widths with a convolution equation, this model is then scaled to match the observed MBA (Figures 4a–4d). Filtering results in a smoothed version of the thermal model increasing the RMBA over the axis (Figures 4e and 4f) and thinning of the axial crust (Figure 4i–4l). The wider the filter (gate), the wider the smoothing and the flatter and broader the filtered thermal model becomes. The width of the filter can be interpreted as a proxy for the cross-axis width of thinner crust and/or of colder denser shallow mantle (Figure 4m–4p). Note that the narrowest filter produces a close fit to the thermal model at segment s11. The *x*-axis of the plots is crustal age to produce a general example that might be applied to other areas. This simple filtering provides a good approximation for what is observed in the MBA and RMBA. We find that the width of the flattened MBA (i.e., width of the shaded green misfit area in Figure 3a) increases from ~0 at segment s12 near Gala-1 to >100 km at s4, the westernmost segment of the CNSC; the RMBA increases from ~0 mGal to >+40 mGal.

4.3. Possible Causes for Flattening MBA

Causes of the MBA flattening (in the form of thin relative crustal thickness or flattened thermal subsidence) have been attributed to inappropriately elevated temperatures in a thermal model where hydrothermal circulation may be cooling the lithosphere (e.g., Cochran & Buck, 2001; Wang et al., 2011). Hydrothermal circulation is not accounted for in a hotter axial thermal model and could result in calculated near-axis crustal thickness that is thinner than it really is. It has been suggested that the standard thermal model may not produce a reliable estimate of crustal thickness at a ridge axis (e.g., Cochran & Buck, 2001; Wang et al., 2011).

We present an alternative model to explain the observed westward flattening of the MBA along the CNSC by producing progressively smoothed thermal models (Figures 4a–4d). We suggest that a wider distribution of melt beneath the spreading axis is reflected in the wider zone of colder mantle (colder than the thermal model) schematically depicted at the bottom (Figure 4m-4p). The central (zero-age) column of the standard thermal model has the highest temperature (1350°K, the temperature of mantle melt; Turcotte & Schubert, 2014) and is associated with the lowest density and lowest MBA (red lines in Figure 3a). If the zero-age melt is not confined to just the central column but is distributed about it over a wider distance, the central column would contain less melt, be colder, and have a higher density than in the standard thermal model. If the central column is split apart and replaced by a new column with new melt distributed over the same distance as before, the older (split) central column would have started cooling, but because the column is impregnated by the new batch of distributed melt, its density would increase at a much slower rate.

4.4. Regional RMBA High at EPR

Relative to the standard thermal model, the gravity across the adjacent EPR indicates a regional positive RMBA and anomalously thin crust along the axis (Figures 2a and 2b). The RMBA on the eastern flank of the EPR indicates a wide zone (100–200 km, or ∼2–3 Myr) of increasing crustal thickness away from the EPR axis. This wide zone of crustal thickening is considered unrealistic because processes that could thicken the crust off-axis, for example, lava flows from the axis, off-axis volcanism, intrusion of magma chambers or sills, and underplating are expected to be restricted to a typical width of ∼10 km from the spreading center since melt is focused toward the axis (e.g., Katz et al., 2006; Sempéré et al., 1993). In addition, seismic surveys reveal an average axial crust of ∼5.5 km at 9°42′–9°57′N of the EPR (Aghaei et al., 2014). We suggest that this apparent thinning must be due to a density variation in the shallow mantle. Of interest is that the gradient in the RMBA on the east flank of the EPR-generated crust is similar to that from west to east along the axis of the CNSC, resulting a similar crustal thickening trend (∼0.4 vs. 0.35 km/°, Figure 2c). We speculate that a wide partial melt zone beneath the EPR that partly underlies the Galapagos gore might explain some of the west-east trend in gravity within the gore. The presence of such a wide melt zone beneath the Galapagos triple junction region and the true crustal thickness of the EPR warrants further seismic constraints and investigation.

5. Conclusions

Shipboard gravity data were combined with satellite gravity data to explore patterns in crustal structure and shallow mantle variation in the Galapagos triple junction region. We observe that the cross-CNSC MBA flattens from about ∼96.4°W toward the gore tip, suggesting an increasing width (0 to >100 km) of thin crust or colder, denser shallow mantle. We suggest that the cause of the flattened MBA may be a westward increase in the distribution width of partial melt within the shallow mantle beneath the CNSC axis. To explore the flattening, we apply a smoothing filter to the standard thermal model with different filter widths. The wider the filter the broader the width of partial melt (i.e., the lower the concentration) and the wider the zone of mantle colder than the thermal model. This smoothing filter model could also explain the observed regional RMBA high on the EPR. The RMBA gradient along the CNSC axis is similar to the gradient extending eastward from the EPR. The gravity gradient along the CNSC could in part reflect the influence of the mantle density structure beneath the EPR. Further studies are needed to explore the applicability of the standard thermal model for other ridge axis, and our interpretation at the Galapagos triple junction region.

Data Availability Statement

Gravity results from this study and code for producing filter models in Figure 4 are uploaded to Zenodo (https://doi.org/10.5281/zenodo.7590816).

Acknowledgments
This study benefited from discussions with Brian E. Tucholke, Doug Wilson, Suzanne Carbotte, Fernando Martinez, Bill Chadwick. We thank David Naar for comments and one anonymous reviewer. Maps were drawn with GMT (Wessel & Smith, 1998). This project was funded by the National Science Foundation of China (Nos 42006055, 41890813, 92258303); the Chinese Academy of Sciences (Nos Y4SL021001, 133244KYSB20180029, ISEE2021PY03, 131551KYSB20200021); the Shenzhen Science and Technology Innovation Commission JCYJ20220818100417038, KCXFZ20211020174803005. The R/V *Sally Ride* cruise 1806 was funded by the National Science Foundation with Grants OCE-1558342 and OCE-1558592.

References

Aghaei, O., Nedimović, M. R., Carton, H., Carbotte, S. M., Canales, J. P., & Mutter, J. C. (2014). Crustal thickness and Moho character of the fast-spreading East Pacific Rise from 9°42′N to 9°57′N from poststack-migrated 3-D MCS data. *Geochemistry, Geophysics, Geosystems*, *15*(3), 634–657. https://doi.org/10.1002/2013GC005069

Bird, P. (2003). An updated digital model of plate boundaries. *Geochemistry, Geophysics, Geosystems*, *4*(3), 101–112. https://doi.org/10.1029/2001GC000252

Canales, J. P., Dañobeitia, J. J., Detrick, R. S., Hooft, E. E. E., Bartolomé, R., & Naar, D. F. (1997). Variations in axial morphology along the Galápagos spreading center and the influence of the Galápagos hotspot. *Journal of Geophysical Research*, *102*(B12), 27341–27354. https://doi.org/10.1029/97JB01633

Canales, J. P., Ito, G., Detrick, R. S., & Sinton, J. (2002). Crustal thickness along the western Galápagos Spreading Center and the compensation of the Galápagos hotspot swell. *Earth and Planetary Science Letters*, *203*(1), 311–327. https://doi.org/10.1016/s0012-821x(02)00843-9

Cochran, J. R., & Buck, W. R. (2001). Near-axis subsidence rates, hydrothermal circulation, and thermal structure of mid-ocean ridge crests. *Journal of Geophysical Research*, *106*(B9), 19233–19258. https://doi.org/10.1029/2001JB000379

DeMets, C., Gordon, R. G., & Argus, D. F. (2010). Geologically current plate motions. *Geophysical Journal International*, *181*(1), 1–80. https://doi.org/10.1111/j.1365-246X.2009.04491.x

Detrick, R. S., Sinton, J. M., Ito, G., Canales, J. P., Behn, M., Blacic, T., et al. (2002). Correlated geophysical, geochemical, and volcanological manifestations of plume-ridge interaction along the Galápagos Spreading Center. *Geochemistry, Geophysics, Geosystems*, *3*(10), 1–14. https://doi.org/10.1029/2002GC000350

Francheteau, J., Armijo, R., Cheminée, J. L., Hekinian, R., Lonsdale, P., & Blum, N. (1990). 1 Ma East Pacific Rise oceanic crust and uppermost mantle exposed by rifting in Hess Deep (equatorial Pacific Ocean). *Earth and Planetary Science Letters*, *101*(2), 281–295. https://doi.org/10.1016/0012-821X(90)90160-Y

Gillis, K. M., Snow, J. E., Klaus, A., Abe, N., Adrião, Á. B., Akizawa, N., et al. (2014). Primitive layered gabbros from fast-spreading lower oceanic crust. *Nature*, *505*(7428), 204–207. https://doi.org/10.1038/nature12778

Holden, J. C., & Dietz, R. S. (1972). Galapagos gore, NazCoPac triple junction and Carnegie/Cocos ridges. *Nature*, *235*(5336), 266–269. https://doi.org/10.1038/235266a0

Ito, G., & Lin, J. (1995a). Mantle temperature anomalies along the present and paleoaxes of the Galápagos spreading center as inferred from gravity analyses. *Journal of Geophysical Research*, *100*(B3), 3733–3745. https://doi.org/10.1029/94jb02594

Ito, G., & Lin, J. (1995b). Oceanic spreading center–hotspot interactions: Constraints from along-isochron bathymetric and gravity anomalies. *Geology*, *23*(7), 657–660. https://doi.org/10.1130/0091-7613(1995)023<0657:OSCHIC>2.3.CO;2

Ito, G., Lin, J., & Gable, C. W. (1997). Interaction of mantle plumes and migrating mid-ocean ridges: Implications for the Galápagos plume-ridge system. *Journal of Geophysical Research*, *102*(B7), 15403–15417. https://doi.org/10.1029/97jb01049

Katz, R. F., Spiegelman, M., & Holtzman, B. (2006). The dynamics of melt and shear localization in partially molten aggregates. *Nature*, *442*(7103), 676–679. https://doi.org/10.1038/nature05039

Lin, J., & Phipps Morgan, J. (1992). The spreading rate dependence of three-dimensional mid-ocean ridge gravity structure. *Geophysical Research Letters*, *19*(1), 13–16. https://doi.org/10.1029/91gl03041

Lonsdale, P. (1988). Structural pattern of the Galapagos microplate and evolution of the Galapagos triple junctions. *Journal of Geophysical Research*, *93*(B11), 13551–13574. https://doi.org/10.1029/JB093iB11p13551

Müller, R. D., Cannon, J., Qin, X., Watson, R. J., Gurnis, M., Williams, S., et al. (2018). GPlates: Building a virtual Earth through deep time. *Geochemistry, Geophysics, Geosystems*, *19*(7), 2243–2261. https://doi.org/10.1029/2018GC007584

Ogg, J. G. (2012). Geomagnetic polarity time scale. In F. M. Gradstein, et al. (Eds.), *The geologic time scale 2012* (pp. 85–113). Elsevier B. V. https://doi.org/10.1016/B978-0-444-59425-9.00005-6

Parker, R. (1972). The rapid calculation of potential anomalies. *Geophysical Journal International*, *31*(4), 447–455. https://doi.org/10.1111/j.1365-246X.1973.tb06513.x

Puchelt, H., & Emmermann, R. (1983). Petrogenetic implications of tholeiitic basalt glasses from the East Pacific Rise and the Galápagos Spreading Center. *Chemical Geology*, *38*(1–2), 39–56. https://doi.org/10.1016/0009-2541(83)90044-X

Ryan, W. B. F., Carbotte, S. M., Coplan, J. O., O'Hara, S., Melkonian, A., Arko, R., et al. (2009). Global Multi-Resolution Topography synthesis. *Geochemistry, Geophysics, Geosystems*, *10*(3), Q03014. https://doi.org/10.1029/2008GC002332

Sandwell, D. T., Müller, R. D., Smith, W. H., Garcia, E., & Francis, R. (2014). New global marine gravity model from CryoSat-2 and Jason-1 reveals buried tectonic structure. *Science*, *346*(6205), 65–67. https://doi.org/10.1126/science.1258213

Schilling, J. G., Fontignie, D., Blichert-Toft, J., Kingsley, R., & Tomza, U. (2003). Pb-Hf-Nd-Sr isotope variations along the Galapagos Spreading Center (101°–83°W): Constraints on the dispersal of the Galapagos mantle plume. *Geochemistry, Geophysics, Geosystems*, *4*(10), 8512. https://doi.org/10.1029/2002GC000495

Schilling, J. G., Kingsley, R. H., & Devine, J. D. (1982). Galapagos hot spot-spreading center system: 1. Spatial petrological and geochemical variations (83°W–101°W). *Journal of Geophysical Research*, *87*(B7), 5593–5610. https://doi.org/10.1029/JB087iB07p05593

Schouten, H., Smith, D. K., Montési, L. G. J., Zhu, W., & Klein, E. M. (2008). Cracking of lithosphere north of the Galapagos triple junction. *Geology*, *36*(5), 339–342. https://doi.org/10.1130/G24431A.1

Searle, R. C., & Francheteau, J. (1986). Morphology and tectonics of the Galapagos Triple Junction. *Marine Geophysical Researches*, *8*(2), 95–129. https://doi.org/10.1007/BF00338224

Sempéré, J. C., Lin, J., Brown, H. S., Schouten, H., & Purdy, G. M. (1993). Segmentation and morphotectonic variations along a slow-spreading center: The Mid-Atlantic Ridge (24°00′N–30°40′N). *Marine Geophysical Researches*, *15*(3), 153–200. https://doi.org/10.1007/BF01204232

Sinton, J., Detrick, R., Canales, J. P., Ito, G., & Behn, M. (2003). Morphology and segmentation of the western Galápagos Spreading Center, 90.5°–98°W: Plume-ridge interaction at an intermediate spreading ridge. *Geochemistry, Geophysics, Geosystems*, *4*(12), 8515. https://doi.org/10.1029/2003GC000609

Smith, D. K., & Schouten, H. (2018). Opening of Hess Deep rift at the Galapagos triple junction. *Geophysical Research Letters*, *45*(9), 3942–3950. https://doi.org/10.1029/2018GL077555

Smith, D. K., Schouten, H., Montési, L., & Zhu, W. (2013). The recent history of the Galapagos triple junction preserved on the Pacific plate. *Earth and Planetary Science Letters*, *371*(2), 6–15. https://doi.org/10.1016/j.epsl.2013.04.018

Smith, D. K., Schouten, H., Parnell-Turner, R., Klein, E. M., Cann, J., Dunham, C., et al. (2020). The evolution of seafloor spreading behind the tip of the westward propagating Cocos-Nazca spreading center. *Geochemistry, Geophysics, Geosystems*, *21*(6), e2020GC008957. https://doi.org/10.1029/2020GC008957

Smith, D. K., Schouten, H., Zhu, W. L., Montési, L. G. J., & Cann, J. R. (2011). Distributed deformation ahead of the Cocos-Nazca Rift at the Galapagos triple junction. *Geochemistry, Geophysics, Geosystems*, *12*(11), 148–151. https://doi.org/10.1029/2011GC003689

Stewart, M. A., Klein, E. M., & Karson, J. A. (2002). Geochemistry of dikes and lavas from the north wall of the Hess Deep Rift: Insights into the four-dimensional character of crustal construction at fast spreading mid-ocean ridges. *Journal of Geophysical Research*, *107*(B10), EPM4-1–EPM4-24. https://doi.org/10.1029/2001jb000545

Stewart, M. A., Klein, E. M., Karson, J. A., & Brophy, J. G. (2003). Geochemical relationships between dikes and lavas at the Hess Deep Rift: Implications for magma eruptibility. *Journal of Geophysical Research*, *108*(B4), 2184. https://doi.org/10.1029/2001JB001622

Tozer, B., Sandwell, D. T., Smith, W. H. F., Olson, C., Beale, J. R., & Wessel, P. (2019). Global bathymetry and topography at 15 arc sec: SRTM15+. *Earth and Space Science*, *6*(10), 1847–1864. https://doi.org/10.1029/2019EA000658

Turcotte, D., & Schubert, G. (2014). *Geodynamics* (3 ed.). Cambridge University Press. https://doi.org/10.1017/CBO9780511843877

Wang, T., Lin, J., Tucholke, B., & Chen, Y. J. (2011). Crustal thickness anomalies in the North Atlantic Ocean basin from gravity analysis. *Geochemistry, Geophysics, Geosystems*, *12*(3), Q0AE02. https://doi.org/10.1029/2010GC003402

Wessel, P., & Smith, W. H. (1998). New, improved version of Generic Mapping Tools released. *Eos, Transactions American Geophysical Union*, *79*(47), 579. https://doi.org/10.1029/98EO00426

Zonenshain, L., Kogan, L., Savostin, L., Golmstock, A. J., & Gorodnitskii, A. (1980). Tectonics, crustal structure and evolution of the Galapagos triple junction. *Marine Geology*, *37*(3–4), 209–230. https://doi.org/10.1016/0025-3227(80)90102-4